Quest Journals
Journal of Research in Mechanical Engineering
Volume 11 ~ Issue 3 (May – June 2025) pp: 11-19
ISSN(Online):2321-8185
www.questjournals.org

Research Paper

A New Approach to Finite Element Modeling of Ultrasonic Transducers

Viet Dung Luong
Faculty of Mechanical Engineering, Thai Nguyen University of Technology, Vietnam

ABSTRACT: *This paper presents a new method for constructing finite element models (FEM) for ultrasonic transducers, aiming to improve the simulation accuracy and efficiency. The proposed method focuses on accurately modeling the interaction between structural components such as the piezoelectric layer, electrode layer, and wave transmission layer with the surrounding environment, while considering factors such as the piezoelectric effect, reflected wave, and energy loss in the material. The finite element model is built for 2D and 3D models, taking into account the influence of meshing on the simulation results, especially the meshing of ceramic material plates. The simulation results are compared with standard data, showing that the new FEM model achieves high accuracy in predicting the frequency characteristics and impulse response of ultrasonic transducers. This proposed method opens up potential applications in the design and optimization of ultrasonic transducers.*

KEYWORDS: *Transducer, Finite element, Simulation, Ceramic*

R*eceived 25 May., 2025;* ***R****evised 06 June., 2025;* ***A****ccepted 08 June., 2025*

I. INTRODUCTION

Nowadays, ultrasonic vibration plays an increasingly pivotal role in many fields [1]–[4]. In an ultrasonic vibration generation system, the vibration head plays a vital role. It consists of a transducer, booster, and model components. The performance of this device depends heavily on the complex interaction between its mechanical, electrical, and acoustic properties. Therefore, accurate modeling of the ultrasonic head is crucial for optimizing the design and achieving the expected performance. Up to now, numerous studies have addressed the design and optimization of ultrasonic transducers for various applications. For instance, Xuan Li et al. proposed a modified ultrasonic vibration device tailored for rock drilling systems, where compact size and high performance are critical requirements [5]. Similarly, Mathieson Andrew adapted the design parameters of a conventional Langevin transducer to develop a device suitable for bone surgery, enhancing its applicability in medical procedures [6]. In addition to these efforts, several other works [7]–[13] have also focused on the development of ultrasonic transducers, each optimized for specific operational contexts and performance goals. Finite element analysis (FEA) has emerged as a powerful tool for simulating the complex behavior of ultrasonic transducers, allowing detailed analysis of wave propagation, electromechanical coupling, and acoustic impedance matching. However, conventional FEA methods often face challenges in capturing multi-physics interactions and difficulties in accurately modeling layered structures or damping effects.

In this work, we propose a novel method for finite element modeling of ultrasonic transducers that addresses some of these challenges. Our method emphasizes improved computational efficiency, better representation of material interfaces, and enhanced integration of piezoelectric domains. By validating the model against benchmark results, it has been demonstrated to provide reliable insights into the behavior of the transducer under a wide range of operating conditions. This paper consists of the following sections: Section 1 presents an overview of published studies related to ultrasonic vibrator heads; Section 2 presents a summary of relevant modeling techniques; Section 3 discusses simulation and validation results; and finally, Section 4 concludes the study with key findings and directions for future work.

II. METHODOLOGY

A transducer is a device that converts electrical energy into mechanical energy. In the structure of the transducer, ceramic plates play a central role, so when building a finite element model, it is necessary to pay attention to issues related to ceramic plates.

2.1. ELECTROMECHANICAL RELATIONSHIPS OF PIEZOELECTRIC CERAMIC MATERIALS

According to the IEEE standard on piezoelectricity, the linear piezoelectric material equations are given by:

$$\begin{Bmatrix} T_1 \\ T_2 \\ T_3 \\ T_4 \\ T_5 \\ T_6 \\ D_1 \\ D_2 \\ D_3 \end{Bmatrix} = \begin{bmatrix} c_{11}^E & c_{12}^E & c_{13}^E & 0 & 0 & 0 & 0 & 0 & -e_{31} \\ c_{12}^E & c_{22}^E & c_{23}^E & 0 & 0 & 0 & 0 & 0 & -e_{32} \\ c_{13}^E & c_{23}^E & c_{33}^E & 0 & 0 & 0 & 0 & 0 & -e_{33} \\ 0 & 0 & 0 & c_{44}^E & 0 & 0 & 0 & -e_{24} & 0 \\ 0 & 0 & 0 & 0 & c_{55}^E & 0 & -e_{15} & 0 & 0 \\ 0 & 0 & 0 & 0 & 0 & c_{66}^E & 0 & 0 & 0 \\ 0 & 0 & 0 & 0 & e_{15} & 0 & \varepsilon_{11}^S & 0 & 0 \\ 0 & 0 & 0 & e_{24} & 0 & 0 & 0 & \varepsilon_{22}^S & 0 \\ e_{31} & e_{32} & e_{33} & & 0 & 0 & 0 & 0 & \varepsilon_{33}^S \end{bmatrix} \begin{Bmatrix} S_1 \\ S_2 \\ S_3 \\ S_4 \\ S_5 \\ S_6 \\ E_1 \\ E_2 \\ E_3 \end{Bmatrix} \tag{1}$$

where E_i and D_i are the components of the electric field vector and electric field displacement vector, T_i and S_i are the components of the stress and strain vectors:

$$\begin{cases} T = c^E S - e^T E \\ D = eS + \varepsilon^S E \end{cases} \tag{2}$$

where c^E, ε^S are the elastic stiffness matrix and the dielectric constant matrix, respectively; the subscripts E stand for constant electric field and S represent constant strain; e is the piezoelectric constant matrix, representing the electromechanical coupling of the material. This system of equations shows that when the material deforms, an electric field displacement D will be created, and when there is an electric field, an internal stress will be generated. This is consistent with the operating conditions around the resonance point of the ultrasonic vibrator, where the oscillation strain is relatively small, ε^S:

$$\begin{cases} S = s^E T + d^T E \\ D = dT + \varepsilon^T E \end{cases} \tag{3}$$

These quantities have the following corresponding relationships:

$$\begin{cases} [s^E] = [c^E]^{-1} \\ [s^E] = [c^E]^{-1} \\ [\varepsilon^S] = [\varepsilon^T] - [d][e]^T \end{cases} \tag{4}$$

The piezoelectric coefficients are presented in the matrix [d], which represents the coupling between strain and electric field, characteristic for each piezoelectric material. The coefficient matrix of the piezoelectric ceramic (PZT) material with polarization in the z direction (3-direction) is:

$$[d] = \begin{bmatrix} 0 & 0 & 0 & 0 & d_{15} & 0 \\ 0 & 0 & 0 & d_{24} & 0 & 0 \\ d_{31} & d_{32} & d_{33} & 0 & 0 & 0 \end{bmatrix} \tag{5}$$

In which $d_{31} = d_{32}$, $d_{15} = d_{24}$ for normal PZT material, is isotropic in the plane perpendicular to the polarization direction. The constitutive equations for the plane strain response (S_2, S_4, $S_6 = 0$) of a piezoelectric ceramic with a polarization axis coplanar with the 3-axis and hexagonal symmetry around the 3-axis can be expressed as follows[14]:

$$\begin{Bmatrix} T_1 \\ T_3 \\ T_5 \\ D_1 \\ D_3 \end{Bmatrix} = \begin{bmatrix} c_{11}^E & c_{13}^E & 0 & 0 & -e_{31} \\ c_{13}^E & c_{33}^E & 0 & 0 & -e_{33} \\ 0 & 0 & 2c_{44}^E & -e_{15} & 0 \\ 0 & 0 & 2e_{15} & \varepsilon_{11}^S & 0 \\ e_{31} & e_{33} & 0 & 0 & \varepsilon_{33}^S \end{bmatrix} \begin{Bmatrix} S_1 \\ S_3 \\ S_5 \\ E_1 \\ E_3 \end{Bmatrix} \tag{6}$$

The relationship between the electric field E and the electric potential Ø:

$$E = -grad\ \emptyset \tag{7}$$

II.2. ELECTROMECHANICAL RELATIONSHIP OF PIEZOELECTRIC CERAMIC MATERIALS IN FEM

In finite element analysis for PZT materials, it is very important to determine the nodes of each element, including the mechanical displacement vector u and the electric field potential vector $\hat{\phi}$. To determine the continuous mechanical and electrical quantities from the values at the nodes, it is necessary to use the polynomial interpolation functions Nu and NØ [15]. Applying the transformations from equations (1) and (2), we can obtain the following finite element equation system:

$$\begin{cases} m\ddot{u} + d_{uu}\dot{u} + k_{uu}\dot{u} + k_{u\emptyset}\widehat{\emptyset} = f \\ k_{u\emptyset}^{t}u + k_{\emptyset\emptyset}\widehat{\emptyset} = \widehat{Q} \end{cases} \tag{8}$$

where: $\ddot{u},\dot{u}$ are the acceleration vectors and nodal velocity vectors of the elements; k_{uu} is the element stiffness matrix; d_{uu} is the damping matrix; $k_{u\emptyset}$ is the piezoelectric coupling matrix; $k_{\emptyset\emptyset}$ is the dielectric stiffness matrix; m is the mass matrix; f, Q are the mechanical force and charge vectors, respectively, including volume, surface and point distribution quantities.

The damping matrix d_{uu} represents the influence of the degree of deformation loss or mechanical displacement of the material (Rayleigh damping), expressed by the following formula:

$$d_{uu} = \alpha^{(e)} \iiint_{V_e} \rho N_u^t N_u dV + \beta^{(e)} \iiint_{V_e} B_u^t c^E B_u dV = \alpha^{(e)} m + \beta^{(e)} k_{uu} \tag{9}$$

where α and β are the Rayleigh coefficients, which indicate the influence of the mass and stiffness matrices, respectively. Depending on the values of the coefficients α and β, four different damping cases can be distinguished:

- α = 0, β = 0: case of no attenuation
- α = 0, β > 0: viscous damping or attenuation only proportional to stiffness
- α > 0, β = 0: viscous damping or attenuation only proportional to mass
- α > 0, β > 0: viscous damping or total Rayleigh attenuation

The Rayleigh coefficients are determined from the damping ratio for two unequal frequencies ω_i and the damping coefficient ξ_i of the corresponding vibration, according to the following equation [91]

$$\alpha + \beta\omega_i^2 = 2\omega_i\xi_i \tag{10}$$

However, in simulation problems, numerical calculations in design, the oscillation frequencies and damping ratios are often not known in advance. Furthermore, many structures or materials are viscously damped (α = 0). Therefore, the constant β can be determined by expression (4.10) for isotropic materials [97] and the following expression for piezoelectric materials:

$$\beta = {}^{1}/_{\omega_r Q_m} \tag{11}$$

Where ωr is the resonance angular frequency of the vibration mode and Q_m is the mechanical quality factor. The mechanical quality factor can be declared by the manufacturer [16] or determined by an electrical impedance analyzer through the resonance frequency fr and the two frequencies f_1, f_2 corresponding to the frequencies where the impedance amplitude is 3dB less than the resonance value:

$$Q_m = \frac{f_r}{f_1 - f_1} \tag{12}$$

The loss constant β for the piezoelectric ceramic (4.11) can be set directly in the CAE interface of the FEA software. In Abaqus [17], the user can choose to model the damping using the damping properties of the material. The damping matrix is proportional to the viscosity, mass and/or stiffness, and will include the Rayleigh damping coefficients of the material. The overall viscous damping matrix of the material can be written as:

$$D_{viscous} = \sum_{el=1}^{nel} \int_{Ve} \alpha_R^e N_u^t N_u \rho dV + \sum_{el=1}^{nel} \int_{Ve} \beta_R^e B_u^t c^E B_u dV \tag{13}$$

The overall element equation system (after element coupling) of the PZT medium is described by a system of linear differential equations with vectors U and Ø as global variables at the nodes of the mesh, expressed as follows:

$$\begin{cases} M\ddot{U} + D_{uu}\dot{U} + K_{uu}\dot{U} + K_{u\emptyset}\emptyset = F \\ K_{u\emptyset}^{t}U + K_{\emptyset\emptyset}\emptyset = Q \end{cases} \tag{14}$$

where:

$$M = \sum_{el=1}^{nel} \int_{Ve} N_u^t N_u \rho dV$$ Overall mass matrix

$$K_{uu} = \sum_{el=1}^{nel} \int_{Ve} (\nabla N_u)^t c^E (\nabla N_u) dV$$ Overall stiffness matrix

$$K_{u\emptyset} = \sum_{el=1}^{nel} \int_{Ve} (\nabla N_u)^t e^t (\nabla N_\emptyset) dV$$ Overall electromechanical coupling matrix

$$K_{\emptyset\emptyset} = \sum_{el=1}^{nel} \int_{Ve} (\nabla N_\emptyset)^t \varepsilon^S (\nabla N_\emptyset) dV$$ Overall dielectric stiffness matrix

F and Q are the total force and the charge vector, respectively. The system of equations (14) is a semi-discrete finite element system, in which space is discrete and time is continuous.

2.3. Finite element model construction for vibrator

In this study, Herrmann Ultrasonic transducer – Ultraschall 20 kHz, 20/4000 KO Converter – Transducer Schwinger Konvertern is the research object. The technical parameters are presented in Table 1. The detailed dimensions of the vibrator are shown in Figure 1.

Table 1. Parameters of the transducer

Parameter	Unit	Value
Resonant frequency	kHz	20
Power	W	2000
Outer diameter of PZT-8 ring	mm	50
Inner diameter of PZT-8 ring	mm	17
Number of piezoelectric rings	-	4
Design oscillation amplitude	μm	10

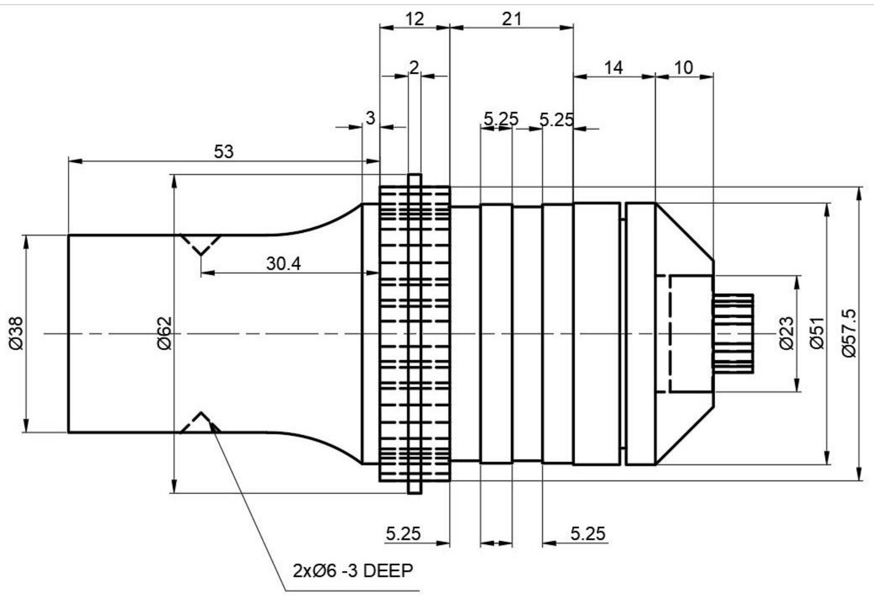

Figure 1. Ultrasonic transducer size

The 2D and 3D ultrasonic vibration head models were created in Abaqus software as shown in Figures 2a, 2b.

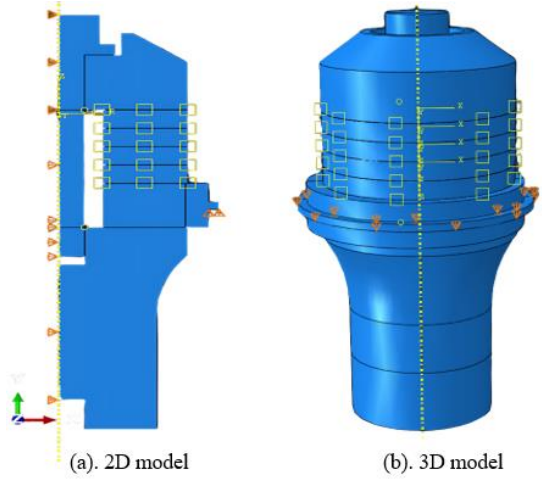

Figure 2. Diagramming of links on models

❖ ***Element Model and Element Mesh***

In the 2D axisymmetric model, the CAX8E element – an axisymmetric quadratic element with 8 nodes – is used for the piezoelectric ceramic parts and CAX8 is used for the rest of the vibrator parts (Figure 3).

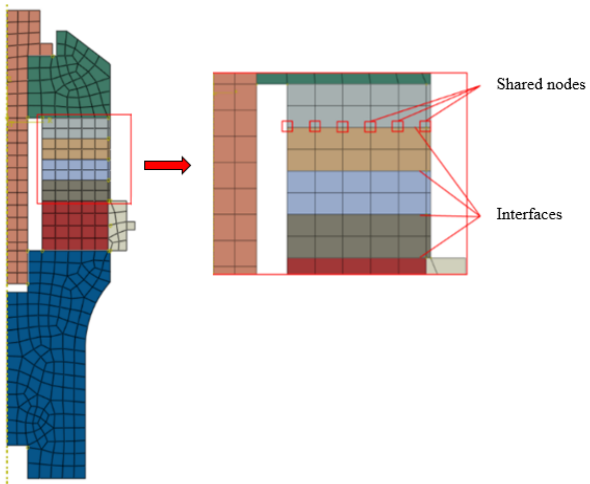

Figure 3. Element mesh diagram in a 2D model

In the 3D model, a quadratic solid element with 20 nodes (C3D20) in Abaqus is used. This type of element allows for efficient simulation of complex geometries as well as large deformation states. In addition, C3D20 can also simulate a variety of material properties such as linear and nonlinear elasticity, plastic deformation, or damage, suitable for many types of engineering problems in fields such as aerospace, mechanical engineering, or civil engineering. Compared with first-order elements, C3D20 elements provide faster convergence and higher numerical stability in analyses with high accuracy requirements. In this study, two types of elements, C3D20R (integral reduction) and C3D20E (electric effects included), are selected to perform modal analysis for the ultrasonic vibrator model (Figure 4).

To ensure the accuracy of numerical simulation as well as the ability to faithfully reflect the mechanical-vibration characteristics of the ultrasonic vibrator, the meshing process must comply with the following technical requirements:

- ✓ Local mesh density increases at complex load-bearing or contact areas;
- ✓ Locations such as the interface between PZT layers, front-back guide blocks, and tightening bolts require thicker meshes to accurately capture local deformation and stress concentrations;
- ✓ Use smaller elements at mechanical focal points or material boundaries with large elastic modulus differences;
- ✓ Reasonable element geometry and uniform expansion ratio;
- ✓ Elements should have reasonable aspect ratios, avoiding excessive elongation in one direction (high aspect ratio), especially in PZT blocks, to avoid distorting transmitted ultrasonic waves;
- ✓ Prefer square or quasi-equilateral mesh elements to ensure numerical stability;
- ✓ Node-to-node contact at fixed interfaces

- ✓ Contact surfaces between overlapping components (PZT - guide blocks - bolts) should be meshed with matching nodes.
- ✓ To achieve efficient node-to-node contact, it is necessary to design precise geometry and use uniform meshing techniques at the interfaces.
- ✓ Reduce mesh density in less affected areas to optimize computational resources.
- ✓ Blocks far from the main active area (e.g., the end of the following block) can use larger elements to reduce computation time without affecting the overall results;
- ✓ Optimize element orientation in the main oscillation direction;
- ✓ In axial oscillation problems, element orientation should be prioritized in the Y or Z axis direction (depending on the axis system), to better describe the propagating wave.

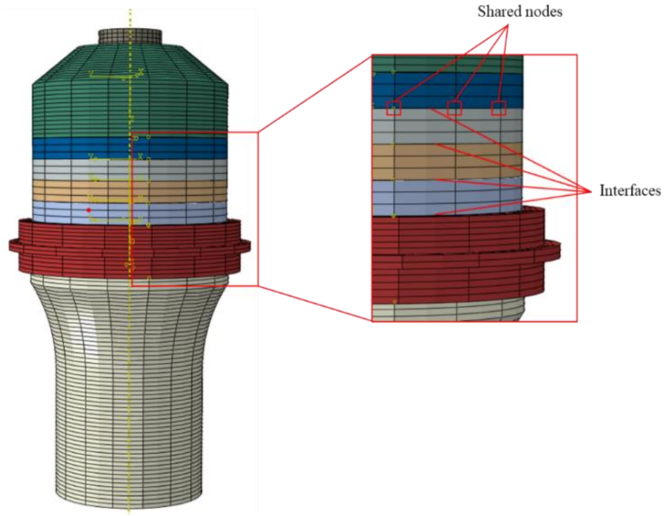

Figure 4. Element meshing diagram in a 3D model

III. RESULTS AND DISCUSSION

The material specifications of the Herrmann Ultrasonic converter parts are shown in the following table 2. The element types and meshing are shown in Table 3.

Table 2. Material parameters in the finite element model

Detail	Material	Density (g/cm^3)
Back mass	Inconel 718	8,24
Ceramic PZT	PZT-8	
Intermediate block	Stainless steel ST304	7,930
Belt block	Alloy AL-7075T6	2,81
Front mass	Titanium Ti-6AI-4V	4,43
Bolt	Inconel 718	8,24
Back mass	Inconel 718	8,24

Table 3. Element types and mesh sizes used in 2D and 3D models

	Element type		Mesh size
	PZT	Other details	
2D	CAX8RE	CAX8R	1mm
3D	C3D20RE	C3D20R	1mm

❖ **Natural oscillation problem**

Figure 5a illustrates the axial displacement field distribution (U_2) of the ultrasonic vibrator at the first fundamental mode of vibration, extracted from the natural vibration analysis in an axisymmetric 2D finite element model. The problem is solved by the Lanczos method, which allows for the determination of the natural frequencies and corresponding mode shapes, thereby evaluating the resonance ability and vibration characteristics of the system.

The results obtained from the natural oscillation problem at the first resonant mode (20.290 kHz) are shown by the distribution of the longitudinal displacement U_2 at characteristic points along the structure of the vibrator. The points in the main body of the vibrator, especially the leading block region, have the largest displacement values, with an amplitude of approximately 1.036 mm. Meanwhile, the belt block, which is assumed to be the fixed connection to the body, has the lowest displacement value, at about 0.0377 mm - still higher than expected for ideal boundary conditions.

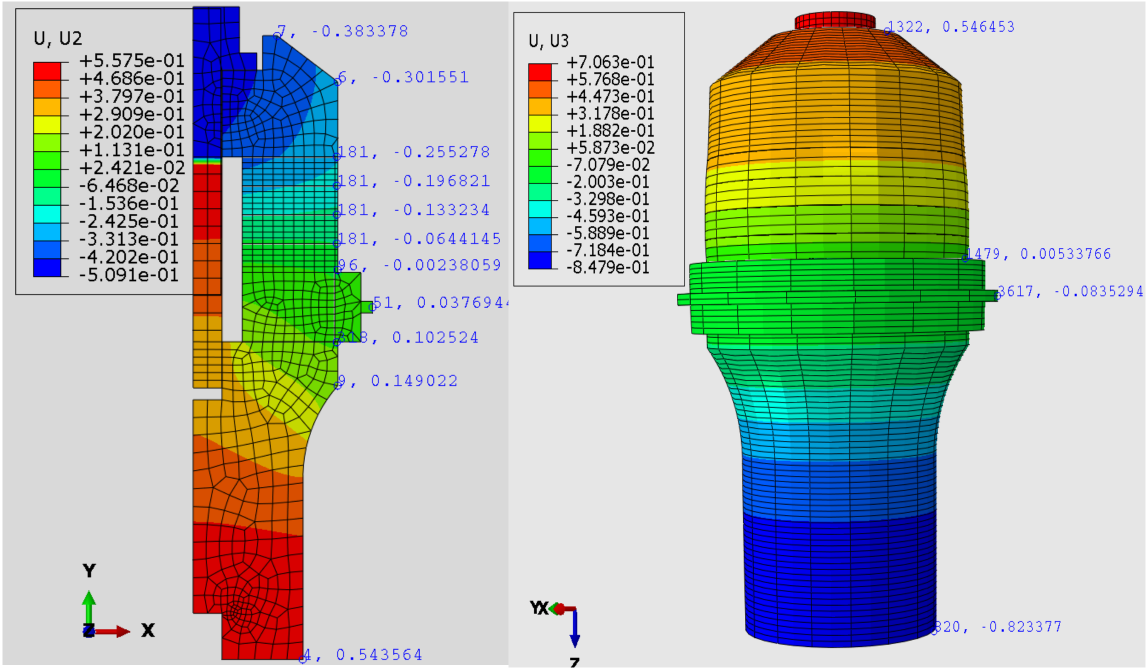

(a) (b)

Figure 5. Axial displacement field distribution in the basic natural vibration mode of 2D and 3D models

Figure 5b shows the longitudinal displacement field distribution U_3 obtained from the natural vibration analysis of the 3D full-body model of the Herrmann vibrator. This is the first fundamental mode of vibration (main mode), corresponding to the first natural resonance frequency of 19,810 Hz (result obtained from the static problem), very close to the target resonance range of the device (20 kHz).

❖ **Forced oscillation problem**

Figure 6a shows the longitudinal displacement field distribution obtained from the forced oscillation problem at the main resonance frequency, using the 2D axially symmetric finite element model of the ultrasonic vibrator. This is the final simulation step in the series of three FEM problems (static - natural oscillation - forced), to evaluate the actual oscillation amplitude response of the transmitter under operating conditions equivalent to the experiment. The results show that the maximum oscillation amplitude reaches nearly 10μm at the top of the leading block, corresponding to the working surface of the device, with a specific value at the P23 measurement point of 0.0099664mm. This figure is almost identical to the value announced by the manufacturer (≈10μm), showing that the model accurately reflects the resonance characteristics and oscillation transmission efficiency of the system. The displacement amplitude is distributed linearly from the belt block (with a value of approximately 0) to the transmitter, clearly showing the basic oscillation mode in the longitudinal direction.

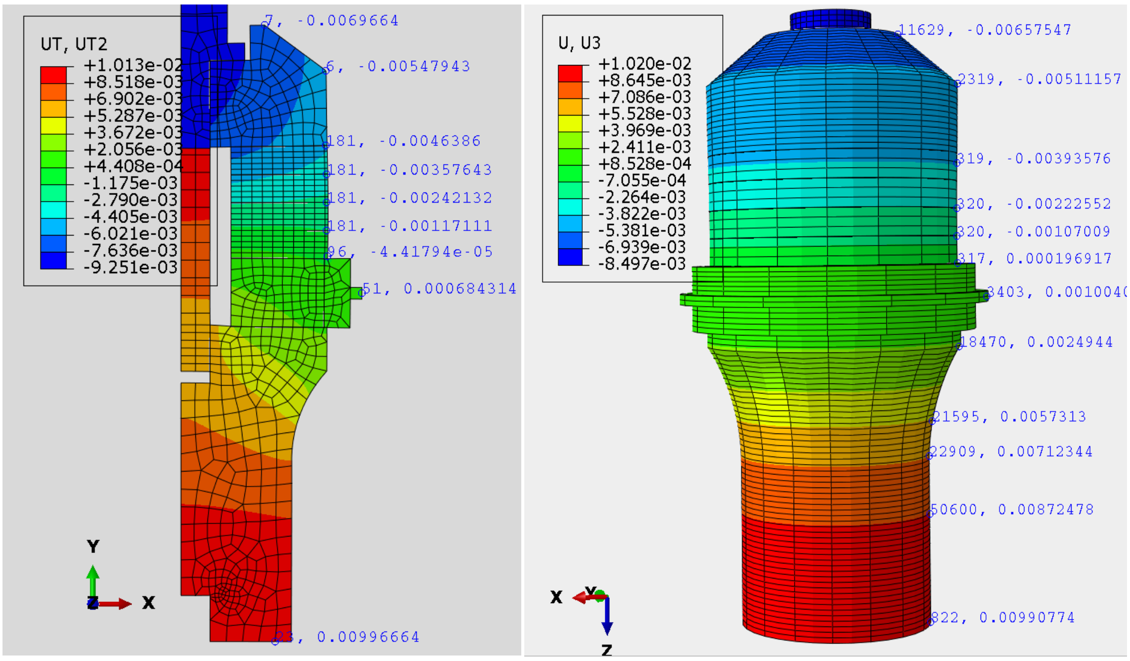

(a) (b)

Figure 6. Axial displacement field distribution at resonance frequency of 2D and 3D models

Figure 6b shows the axial displacement amplitude distribution (U_3) obtained from the forced vibration problem of the 3D finite element model of the ultrasonic vibrator. The results show that the maximum oscillation amplitude reaches about +9.9 µm at the working end. The displacement distribution clearly shows linear variation, with a half-period sine wave form, consistent with the first-order axial resonance mode of the half-wave structure system. This result shows that care must be taken when choosing the ideal oscillation node location in practical designs, and suggests that the booster, rather than the belt block, should be the preferred location for clamping to limit energy dissipation.

IV. CONCLUSION

In this study, a novel finite element modeling method for ultrasonic transducers was proposed to address the major limitations of existing simulation methods. By incorporating more accurate piezoelectric coupling, advanced material damping, or fine meshing techniques, the proposed model improves both the accuracy and efficiency of ultrasonic transducer analysis. The simulation results showed good agreement with the benchmark data provided by the manufacturer. Furthermore, the 2D model provides the flexibility to simulate complex transducer geometries and material properties, making it a valuable tool for both research and industrial applications. Future work will focus on extending this method to model transducer arrays and studying nonlinear effects in high-intensity ultrasonic applications.

REFERENCES

[1] Y. Yao, Y. Pan, and S. Liu, "Power ultrasound and its applications: A state-of-the-art review," *Ultrason. Sonochem.*, vol. 62, 2020, doi: 10.1016/j.ultsonch.2019.104722.

[2] X. Li, P. Harkness, K. Worrall, R. Timoney, and M. Lucas, "A Parametric Study for the Design of an Optimized Ultrasonic Percussive Planetary Drill Tool," *IEEE Trans. Ultrason. Ferroelectr. Freq. Control*, vol. 64, no. 3, pp. 577–589, 2017, doi: 10.1109/TUFFC.2016.2633319.

[3] B. Chandra Behera, "Development and Experimental Study of Machining Parameters in Ultrasonic Vibration-assisted Turning," 2011. [Online]. Available: http://ethesis.nitrkl.ac.in/4416/1/Development_and_experimental_study_of_machining_parameters_in_ultrasonic_vibration-assisted_turning.pdf

[4] A. C. Mathieson, "Nonlinear Characterisation Of Power Ultrasonic Devices Used In Bone Surgery," pp. 1–217, 2012, [Online]. Available: http://theses.gla.ac.uk/3135/

[5] X. Li, M. Lucas, and P. Harkness, "Full and Half-Wavelength Ultrasonic Percussive Drills," *IEEE Transactions on Ultrasonics, Ferroelectrics, and Frequency Control*, vol. 65, no. 11. pp. 2150–2159, 2018. doi: 10.1109/TUFFC.2018.2867535.

[6] A. C. Mathieson, "Nonlinear Characterisation Of Power Ultrasonic Devices Used In Bone Surgery," 2012. [Online]. Available: http://theses.gla.ac.uk/3135/

[7] D. A. DeAngelis, G. W. Schulze, and K. S. Wong, "Optimizing Piezoelectric Stack Preload Bolts in Ultrasonic Transducers," *Phys. Procedia*, vol. 63, pp. 11–20, 2015, doi: 10.1016/j.phpro.2015.03.003.

[8] M. V. Guiman and I. C. Roca, "A New Approach on Vibrating Horns Design," *Shock Vib.*, vol. 2017, 2017, doi: 10.1155/2017/8532021.

[9] E. Evaluation, O. F. Indicators, O. F. Nonlinearity, F. O. R. Use, I. N. Ultrasound, and T. Characterizations, "Experimental Evaluation of Indicators of Nonlinearity," vol. 28, no. 02. pp. 1509–1520, 2002.

[10] M. Hahn, Y. Cho, G. Jang, and B. Kim, "Optimal design and experimental verification of ultrasonic cutting horn for ceramic composite material," *Appl. Sci.*, vol. 11, no. 4, pp. 1–13, 2021, doi: 10.3390/app11041954.

[11] R. Marat-Mendes, C. J. Dias, and J. N. Marat-Mendes, "A comparative study of piezoelectric materials using smart angular accelerometers," in *Key Engineering Materials*, 2002, vol. 230–232, pp. 181–184. doi: 10.4028/www.scientific.net/kem.230-232.181.

[12] H. Razavi, M. Keymanesh, and I. F. Golpayegani, "Analysis of free and forced vibrations of ultrasonic vibrating tools, case study: ultrasonic assisted surface rolling process," *Int. J. Adv. Manuf. Technol.*, vol. 103, no. 5–8, pp. 2725–2737, 2019, doi: 10.1007/s00170-019-03718-x.

[13] S. Sherrit, B. P. Dolgin, Y. Bar-Cohen, D. Pal, J. Kroh, and T. Peterson, "Modeling of horns for sonic/ultrasonic applications," in *Proceedings of the IEEE Ultrasonics Symposium*, 1999, vol. 1, pp. 647–651. doi: 10.1109/ultsym.1999.849482.

[14] "Piezoelectric Ceramics Properties: Technical Guide".

[15] R. Lerch, "Simulation of Piezoelectric Devices by Two- and Three-Dimensional Finite Elements," *IEEE Trans. Ultrason. Ferroelectr. Freq. Control*, vol. 37, no. 3, pp. 233–247, 1990, doi: 10.1109/58.55314.

[16] A. Abdullah, M. Shahini, and A. Pak, "An approach to design a high power piezoelectric ultrasonic transducer," *J. Electroceramics*, vol. 22, no. 4, pp. 369–382, 2009, doi: 10.1007/s10832-007-9408-8.

[17] "Abaqus Analysis User's Guide (6.14)." Accessed: Mar. 25, 2025. [Online]. Available: http://62.108.178.35:2080/v6.14/index.html